Available online at www.sciencedirect.com
ScienceDirect
International Journal of Heat and Fluid Flow 28 (2007) 289–298
International Journal of HEAT AND FLUID FLOW
www.elsevier.com/locate/ijhff

# Three-dimensional natural convection in finned cubical enclosures

Ramón L. Frederick *, Sergio G. Moraga

*Universidad de Chile, Departamento de Ingeniería Mecánica, Casilla 2777, Santiago, Chile*

Received 23 September 2005; accepted 23 March 2006
Available online 15 June 2006

**Abstract**

Three-dimensional natural convection of air in a cubical enclosure with a fin on the hot wall is numerically investigated for Rayleigh numbers of $10^3$–$10^6$. The fin, with a thickness of 1/10 of the cavity side, is placed horizontally on the hot wall. The solid to fluid thermal conductivity ratio ($R_k$) and the fin width are varied. Because the fin is shorter than the cavity side, the cold flow sweeps the lower fin face and the hot wall at the clearances between the fin sides and the lateral walls, where high vertical velocities are reached. The fin inhibits the frontal and lateral access of fluid to the upper fin face, especially at low Rayleigh numbers. Low values of $R_k$ cause heat transfer reductions. The contribution of the fin faces increases at high $R_k$ causing heat transfer enhancements above 20%, which exceed the ones obtained in most two-dimensional studies. In the range of $Ra$ from $10^5$ to $10^6$, maximum heat transfer rates are found for dimensionless fin widths of 0.6 and 0.8 respectively. It is concluded that for $10^5 \leqslant Ra \leqslant 10^6$ a fin of partial width is more effective in promoting heat transfer than a fin of full width.


*Keywords:* Finned cavities; 3D results; Heat transfer enhancement

## 1. Introduction

The literature on heat transfer in fluid filled enclosures with fins attached to the active walls has expanded recently. Several works report simulations of the steady state, laminar, two-dimensional flow and temperature fields in search for ways to control and optimize the overall cavity heat transfer by the addition of fins. Less effort has been devoted to three-dimensional simulations for this situation.

One of the first works on the subject (Bejan, 1983) considered the effect of a fin attached to the hot wall of a differentially heated enclosure filled with a fluid-saturated porous medium. Studies on fluid filled cavities with a single fin are more numerous. Fins of zero thickness (Frederick, 1989; Oosthuizen and Paul, 1985; Nag et al., 1993) and conducting fins with variable thickness have been studied (Frederick and Valencia, 1989; Nag et al., 1994). In square cavities, fins of low thermal conductivity are found to cause small heat transfer reductions, while moderate enhancements have been obtained with fins of high thermal conductivity. Heat transfer rate exhibits asymptotic behaviour for solid to fluid thermal conductivity ratios above 1000 (Nag et al., 1994). Recent papers (Shi and Khodadadi, 2003; Lakhal et al., 1997) have considered the case of infinite thermal conductivity as an upper limit of heat transfer enhancement. Even in this favourable condition, heat transfer is very insensitive to the fin length and vertical position (Shi and Khodadadi, 2003), allowing few opportunities for optimization, as the enhancement is rather moderate. Recent papers, however, report very high heat transfer enhancements and reductions in cavities with thin fins of high and low thermal conductivity respectively (Tasnim and Collins, 2004; Bilgen, 2005). In slender cavities, heat transfer enhancements of about 40% can be reached using multiple fins (Scozia and Frederick, 1991; Lakhal et al., 1997; Yucel and Turkoglu, 1998), because of the circulation cells generated in the microcavities defined by pairs of fins.

In spite of the extensive work on the subject, scarce information is available on the effect of fins on heat transfer in

* Corresponding author. Tel.: +56 2 678 4448; fax: +56 2 698 8453.
*E-mail address:* rfrederi@cec.uchile.cl (R.L. Frederick).

0142-727X/$ - see front matter © 2006 Elsevier Inc. All rights reserved.
doi:10.1016/j.ijheatfluidflow.2006.03.005

**Nomenclature**

| | |
|---|---|
| $b$, $e$ | fin width and thickness respectively, m |
| $g$ | gravity constant, m s$^{-2}$ |
| $k_s$, $k_f$ | thermal conductivities of fin material and air, W/m K |
| $L$ | cavity side, m |
| $Nu$, $\overline{Nu}$ | local and overall Nusselt numbers |
| $Pr$ | Prandtl number, $v/\alpha$ |
| $Ra$ | Rayleigh number, $g\beta\Delta TL^3/v\alpha$ |
| $R_k$ | thermal conductivity ratio, $k_s/k_f$ |
| $s$ | fin length, m |
| $T$ | dimensional temperature field, K |
| $T_{av}$ | average temperature of the active walls, K |
| $T_H$, $T_C$ | hot and cold wall temperatures, K |
| $U$, $V$, $W$ | dimensionless velocities in $X$, $Y$, $Z$ directions |
| $U_m$, $V_m$ | maximum velocities at the axes of the plane $Z = 0.5$ |
| $V_{max}$ | absolute maximum vertical velocity in the enclosure |
| $X$, $Y$, $Z$ | dimensionless coordinates |

*Greek symbols*

| | |
|---|---|
| $\alpha$ | thermal diffusivity of air, m$^2$ s$^{-1}$ |
| $\beta$ | thermal expansion coefficient, K$^{-1}$ |
| $\Delta T$ | overall temperature difference ($T_H - T_C$) |
| $\Theta$ | dimensionless temperature, $(T - T_{av})/(T_H - T_C)$ |
| $v$ | kinematic viscosity of air, m$^2$ s$^{-1}$ |
| $\rho$ | air density, kg m$^{-3}$ |

cubical enclosures. da Silva and Gosselin (2005) report heat transfer enhancements obtained by the use of high thermal conductivity fins of significant volume in that geometry.

Three-dimensionality gives freedom to consider fins of many shapes, dimensions, and locations in search for heat transfer enhancement. A rich variety of flow patterns arises with changes in these parameters. In this paper, we study the flow patterns and heat transfer in a cubical enclosure with two opposite vertical, isothermal active walls and the remaining walls adiabatic. A horizontal conducting fin of parallelepiped shape is fixed mid height on the hot wall. Its smallest dimension (thickness) is vertical. We consider relatively thick fins in order to promote heat transfer. In addition, one is interested in utilizing fins with width ($b$) shorter than the cavity side ($L$), a case in which a fully three-dimensional flow pattern is expected. The cold fluid approaching the fin from below can reach the upper fin face from the fin front edge (as it is in two-dimensional studies) as well as from the sides. It is expected that this flow pattern will provide higher heat transfer rates than the cubical cavity with a fin of $b = L$, as well as with respect to the predictions of two-dimensional simulations that model the latter situation approximately. In the fully three-dimensional situation, the conditions causing heat transfer enhancement or reduction are still unknown, so the sensitivity to the fin thermal conductivity has to be studied. The three-dimensional approach is also useful to describe the heat transfer contributions of the different fin faces, and to explore further possibilities for enhancing cavity heat transfer.

Heat transfer in finned cavities depends on Rayleigh number, Prandtl number, cavity aspect ratio, as well as on a set of fin parameters, such as thermal conductivity, width, shape, length, thickness, and location. No sensitivity analysis will be made here to the last four variables. Previous works report heat transfer reductions when the dimensionless fin thickness decreases from 0.1 to 0.02, and then an increase is observed for thinner fins (Nag et al., 1994; Tasnim and Collins, 2004). Shi and Khodadadi (2003) show that heat transfer is lower with shorter fins and that its growth for perfectly conducting fins is marginal for $s/L > 0.5$. We do not attempt an optimization of heat transfer here because of the high number of variables. However, the results and their physical interpretation can give insight on parameter settings leading to higher heat transfer enhancements. The paper is organized as follows: The flow patterns and heat transfer for a range of Rayleigh numbers will be described in detail for a fin of fixed width ($b < L$), thickness, length and thermal conductivity ratio. Then the sensitivity of heat transfer to changes in $R_k$ and fin width will be examined. Finally, maximum heat transfer rates as a function of fin width will be sought at high Rayleigh numbers.

## 2. Formulation

A cubical cavity of side $L$ contains air ($Pr = 0.71$). A rectangular, conducting fin is centrally attached to the hot wall, as shown in Fig. 1. The hot wall at $X = 0$ is at $T_H$, and the cold wall at $T_C$ ($X = 1$). The remaining four walls are adiabatic. Independent parameters are the Rayleigh and Prandtl numbers, and the dimensionless fin parameters for length, width and thickness ($s/L$, $b/L$, and $e/L$), and the thermal conductivity ratio, $R_k = k_s/k_f$.

With so many independent parameters, for the purposes of this article we choose to vary only the Rayleigh number ($10^3$–$10^6$), the fin thermal conductivity and the dimensionless fin width ($b/L$), which can be varied only in three-dimensional studies. Given the thermal conductivity of air, $R_k$ ratios of 10, 100, and 1000 are chosen to represent solids characterised as a poor insulator, a poor conductor and a metal respectively. The width $b/L$ will initially be given values of 0.5 and 0.7. The ratio $b/L = 1$ corresponds to a full fin width. The other geometrical ratios will be kept constant ($s/L = 0.5$ and $e/L = 0.1$).

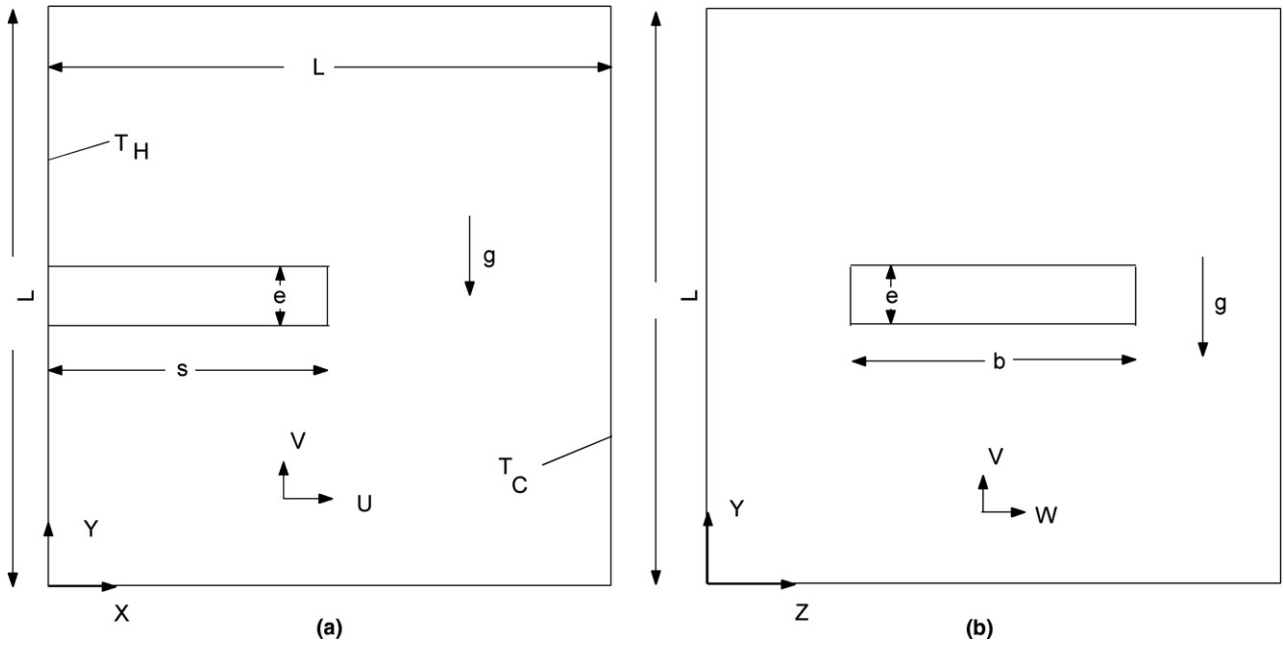


Fig. 1. Physical model and coordinates: (a) plane $Z = 0.5$, (b) plane $X = 0$.

In the specified range of $Ra$, time dependent flow is not expected. The dimensionless equations of continuity (1), momentum (2)–(4) and energy (5) for steady laminar flow of an incompressible fluid with the Boussinesq approximation and with negligible viscous dissipation are respectively:

$$\frac{\partial U}{\partial X}+\frac{\partial V}{\partial Y}+\frac{\partial W}{\partial Z}=0 \tag{1}$$

$$U\frac{\partial U}{\partial X}+V\frac{\partial U}{\partial Y}+W\frac{\partial U}{\partial Z}=-\frac{\partial P}{\partial X}+Pr\left(\frac{\partial^2 U}{\partial X^2}+\frac{\partial^2 U}{\partial Y^2}+\frac{\partial^2 U}{\partial Z^2}\right) \tag{2}$$

$$U\frac{\partial V}{\partial X}+V\frac{\partial V}{\partial Y}+W\frac{\partial V}{\partial Z}=-\frac{\partial P}{\partial Y}+Pr\left(\frac{\partial^2 V}{\partial X^2}+\frac{\partial^2 V}{\partial Y^2}+\frac{\partial^2 V}{\partial Z^2}\right)+Ra\,Pr\Theta \tag{3}$$

$$U\frac{\partial W}{\partial X}+V\frac{\partial W}{\partial Y}+W\frac{\partial W}{\partial Z}=-\frac{\partial P}{\partial Z}+Pr\left(\frac{\partial^2 W}{\partial X^2}+\frac{\partial^2 W}{\partial Y^2}+\frac{\partial^2 W}{\partial Z^2}\right) \tag{4}$$

$$U\frac{\partial \Theta}{\partial X}+V\frac{\partial \Theta}{\partial Y}+W\frac{\partial \Theta}{\partial Z}=\frac{\partial^2 \Theta}{\partial X^2}+\frac{\partial^2 \Theta}{\partial Y^2}+\frac{\partial^2 \Theta}{\partial Z^2} \tag{5}$$

Within the fin itself, the energy equation is

$$\frac{\partial^2 \Theta}{\partial X^2}+\frac{\partial^2 \Theta}{\partial Y^2}+\frac{\partial^2 \Theta}{\partial Z^2}=0 \tag{6}$$

The equations were made dimensionless using $L$, $\alpha$, $\rho$ and $\Delta T$ as reference quantities. The dimensionless velocities $U$, $V$ and $W$ are zero on the cavity walls. The dimensionless temperature $\Theta$ takes values of 0.5 and $-0.5$ at the hot and cold walls respectively.

Zero velocities ($U = V = W = 0$) are specified on the fin faces. These faces are located on the following planes: $X = 0$ (fin base), $X = s/L$ (fin tip), $Y = 0.5 - e/2L$ and $Y = 0.5 + e/2L$ (bottom and top faces), $Z = 0.5 - b/2L$ and $Z = 0.5 + b/2L$ (left and right faces). Adiabatic conditions are $\partial\Theta/\partial Y = 0$ and $\partial\Theta/\partial Z = 0$ on the horizontal and lateral cavity walls. The fin base ($X = 0$) is at $\Theta = 0.5$, while the thermal boundary conditions for the other fin faces (front, sides and horizontal faces) are

$$-R_k\left(\frac{\partial\Theta}{\partial X}\right)_s=-\left(\frac{\partial\Theta}{\partial X}\right)_f \quad \text{at } X=s/L \tag{7}$$

$$-R_k\left(\frac{\partial\Theta}{\partial Y}\right)_s=-\left(\frac{\partial\Theta}{\partial Y}\right)_f \quad \text{at } Y=0.5-e/2L \text{ and } Y=0.5+e/2L \tag{8}$$

$$-R_k\left(\frac{\partial\Theta}{\partial Z}\right)_s=-\left(\frac{\partial\Theta}{\partial Z}\right)_f \quad \text{at } Z=0.5-b/2L \text{ and } Z=0.5-b/2L \tag{9}$$

Subscripts s and f indicate that the gradients are evaluated at the solid and at the fluid side of the interface respectively. Local Nusselt numbers in the air-filled region are evaluated as

$$Nu=U\Theta-\frac{\partial\Theta}{\partial X} \tag{10}$$

Overall Nusselt numbers were computed at the cold wall ($X = 1$), where $U = 0$, at $X = 0.6$ (in the fluid region beyond the fin), and at the hot wall on which the local Nusselt number is computed by Eq. (10) with $X = 0$, $U = 0$, except at the fin base, where it is given by

$$Nu=-R_k\frac{\partial\Theta}{\partial X} \tag{11}$$

Local Nusselt numbers at the fin faces were also calculated. From these Nusselt numbers, the contribution of the fin faces to cavity heat transfer was determined.

## 3. Numerical method

A 3D code based on the SIMPLER method (Patankar, 1980) was used. From it, a 2D code was prepared. Uniform staggered grids of $82^3$, $102^3$ and $122^3$ nodes were tried. As the overall Nusselt numbers evaluated with the two finer grids differed by only 0.09% at $Ra = 10^5$ and by 0.3% at $Ra = 10^6$, the $102^3$ grid was chosen, as the finer one required an excessive computer time. The $102^3$ grid also allows easier specification for the location of fin faces and provides ten temperature nodes across the fin thickness. Nodes of the normal velocity component were placed on cavity walls and fin faces. The temperatures at the two nodes straddling a fin face are linked by diffusive discretisation coefficients that are calculated using the harmonic mean of the diffusive coefficients for air and solid (Patankar, 1980). This procedure allows imposition of the temperature conditions on all fin faces, except on the plane $X = 0$, where the temperature of the hot wall prevails. In interior points of the fin, velocities were defined as zero, but the discretised energy equation was solved for these points. Given the symmetry of the problem with respect to the plane $Z = 0.5$, we solved the system of equations in the region comprised between $0 \leqslant Z \leqslant 0.5$, obtaining time savings in each run.

Overall Nusselt numbers ($\overline{Nu}$) and velocities computed with the code for the case of an unfinned cubical cavity were compared with results from a benchmark solution proposed by Tric et al. (2000). The agreement was good, as overall Nusselt numbers (Table 1), did not differ by more than 0.38% from their results at Rayleigh numbers between $10^3$ and $10^5$. The difference at $Ra = 10^6$ was higher (1.16%). However, maximum velocities on the symmetry plane $Z = 0.5$ did not differ by more than 0.7% from the values of Tric et al. (2000) at any Rayleigh number. Two-dimensional results for an unfinned square cavity were also in excellent agreement with the 2D results of Tric et al. (2000) and De Vahl-Davis (1983). For the case of finned cavities the code was validated by comparing the overall Nusselt numbers at three locations ($X = 0$, 0.6 and 1) finding values that differed only in the third decimal figure. Two-dimensional runs for finned cavities with the parameters used by Nag et al. (1994) gave exact agreement with the results of that work. For consistency, the overall Nusselt numbers given in Table 1 were used to evaluate heat transfer enhancement.

Table 1
Maximum velocities at the axes of plane $Z = 0.5$ and overall Nusselt number for the undivided cubical cavity

| $Ra$ | $U_m$ | $V_m$ | $\overline{Nu}$ |
|---|---|---|---|
| $10^3$ | 3.53358 | 3.54058 | 1.07124 |
| $10^4$ | 16.7011 | 18.6570 | 2.05703 |
| $10^5$ | 37.7008 | 65.4339 | 4.35340 |
| $10^6$ | 68.6887 | 217.9988 | 8.74003 |

## 4. Results and discussion

### 4.1. Flow patterns and temperature fields for $b/L = 0.5$, $R_k = 10$

The main circulation cell at low Rayleigh numbers will be described first, for $Ra = 10^4$. On $XY$ planes near the lateral fin edge the flow is similar to the one observed in undivided cavities, but on the midplane $Z = 0.5$ (Fig. 2a and b),

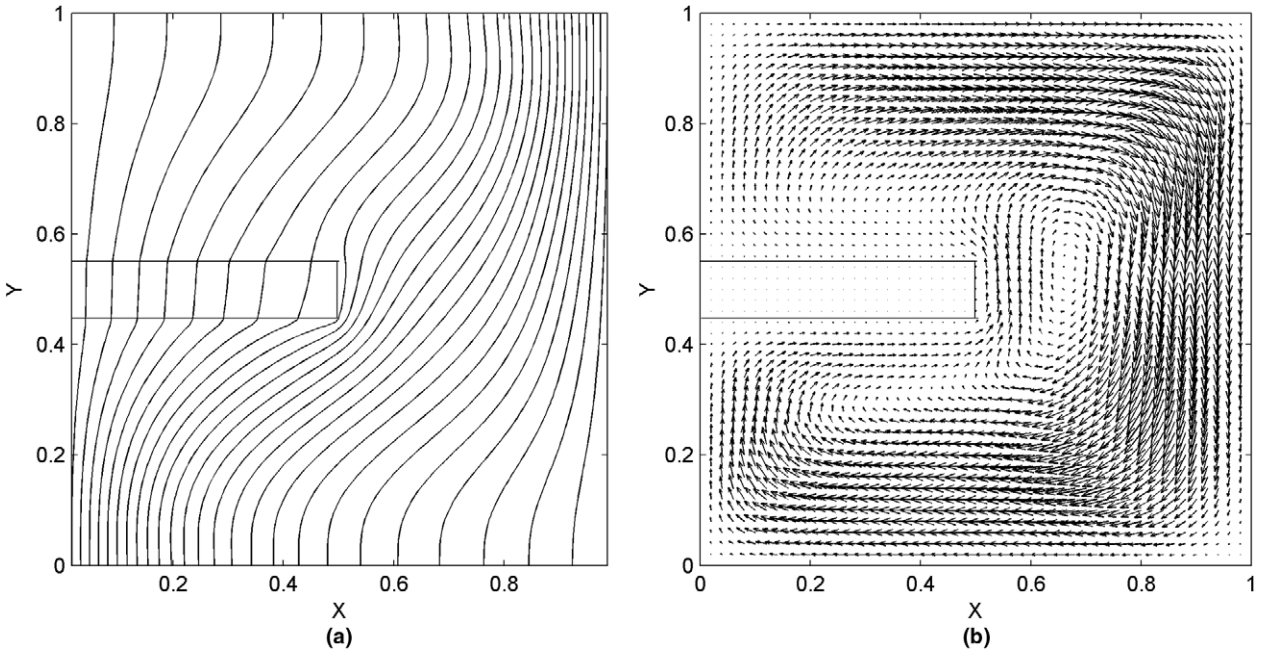


Fig. 2. Isotherms and flow field on $Z = 0.5$, $b/L = 0.5$, $R_k = 10$, $Ra = 10^4$: (a) isotherms, (b) velocity vectors.

Table 2
Maximum velocities ($U_m$, $V_m$) at the axes of plane $Z = 0.5$, for $b/L = 0.5$

| $Ra$ | $U_m$ | | | * |
|---|---|---|---|---|
| | $R_k = 10$ | $R_k = 100$ | $R_k = 1000$ | $R_k = 1000$ |
| $10^3$ | 1.34903 | 1.39304 | 1.40119 | 1.1117 |
| $10^4$ | 9.68584 | 11.0525 | 10.2199 | 8.2942 |
| $10^5$ | 35.9920 | 34.8900 | 33.1655 | 35.3837 |
| $10^6$ | 80.05774 | 89.9006 | 94.0828 | 121.9004 |
| | $V_m$ | | | |
| $10^3$ | 0.48434 | 0.77784 | 0.85362 | 1.2157 |
| $10^4$ | 4.03051 | 7.51660 | 8.24154 | 10.9053 |
| $10^5$ | 18.9820 | 31.9990 | 36.1517 | 43.7038 |
| $10^6$ | 49.0452 | 90.8235 | 106.2730 | 120.4666 |

The column marked with (*) corresponds to $b/L = 0.7$.

the circulation reflects the effect of the fin: cold fluid approaching the hot wall below the fin, sweeps the bottom fin face as it returns. At this $Ra$, no significant part of this stream moves toward the hot wall above the fin, as shown by the isotherms in that region. Instead, it mixes with a loop adjacent to the fin tip, to return to the cold wall. This loop rotates clockwise about a horizontal axis aligned with $Z$, near the fin tip. Fig. 2a and b shows that access of the flow to the active wall above the fin is difficult, a fact that severely limits the local heat transfer rates at that location. The maximum velocities at the axes of the plane $Z = 0.5$, which can be considered representative of the intensity of fluid motion in the cavity, are given in Table 2. Invariably, $U_m$ occurs near the cavity top at $X = 0.5$, $Z = 0.5$, and $V_m$, in front of the fin tip, at $Y = 0.5$, $Z = 0.5$.

At $Ra = 10^3$, the regime is conductive, with nearly vertical isotherms on $Z = 0.5$. As conduction along the fin displaces hot isotherms to the right, the upper and lower fin faces transfer heat to the surrounding cold fluid. At $Ra = 10^4$ (Fig. 2a) the hot wall temperature gradients are high only below the fin. The incipient thermal stratification that would occur without fin at the same $Ra$ is suppressed by the obstacle. Convection suppression creates a nearly stagnant zone in the corner region above the fin near the hot wall, resulting in low temperature gradients at this wall. The vertical temperature gradient on the top fin surface is reversed at this Rayleigh number, i.e. the fluid is transferring heat to the upper fin face. The horizontal temperature gradient is relatively high at the fin tip.

Near the hot wall (plane $X = 0.09$, Fig. 3a) the flow rises at the clearances between the fin sides and the lateral walls ($Z = 0$ and $Z = 1$), where the vertical upward velocities are the highest in the cavity ($V_{max}$, Table 3). Past the fin, this flow continues upwards, deviating slightly toward the cavity midplane $Z = 0.5$, so the lateral velocities above the fin are extremely low. A similar pattern is seen on planes $X > 0.09$, but there, vertical and lateral motion is significant only around the fin. At the fin tip there is a definite upward flow, which is part of the main loop located there. The cold flow, after impinging on the hot wall below the fin moves radially toward the lateral fin edges (Fig. 3b) and continues upwards as seen in Fig. 3a. Immediately above the fin, motion toward the midplane $Z = 0.5$ is noticeable only near the fin edges, not actually reaching the midplane, as is inferred from Figs. 2b and 3a. Further up, at $Y > 0.7$ (Fig. 3a), the heated fluid concentrates to return to the cold wall, without actually sweeping the hot wall and the top fin face significantly.

The above description shows that the blockage of motion by the fin is important for low Rayleigh numbers. However, at $Ra = 10^5$, circulation all around the fin profile

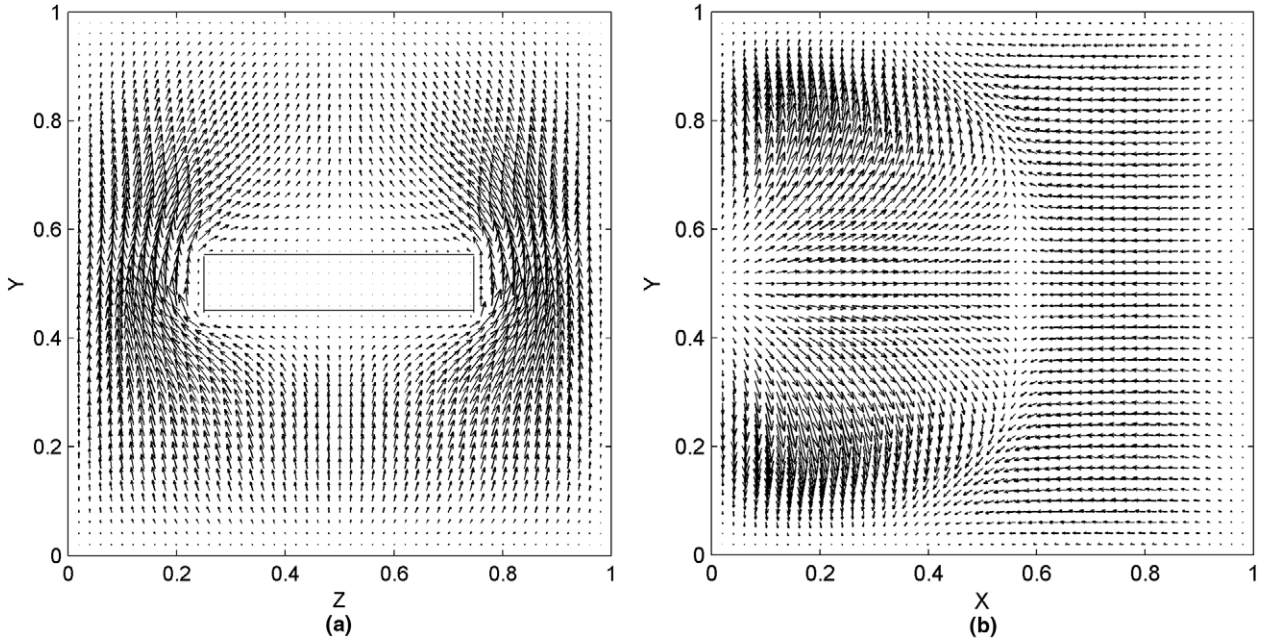


Fig. 3. Velocity vectors on two planes at $Ra = 10^4$, $b/L = 0.5$, $R_k = 10$: (a) $X = 0.09$, (b) $Y = 0.385$.

Table 3
Maximum vertical velocities in the finned cavity at $b/L = 0.5$ and their coordinates

| $Ra$ | $V_{max}$ | $R_k$ | $X$ | $Y$ | $Z$ | $V^*_{max}$ |
|---|---|---|---|---|---|---|
| $10^3$ | 2.3118 | 10 | 0.155 | 0.5 | 0.135 | 1.8771 |
| | 2.2005 | 100 | 0.175 | 0.5 | 0.135 | 1.6550 |
| | 2.1790 | 1000 | 0.185 | 0.5 | 0.135 | 1.7888 |
| $10^4$ | 18.4560 | 10 | 0.155 | 0.5 | 0.135 | 17.5128 |
| | 20.9033 | 100 | 0.145 | 0.49 | 0.135 | 15.7775 |
| | 18.7705 | 1000 | 0.155 | 0.49 | 0.135 | 16.2499 |
| $10^5$ | 90.0902 | 10 | 0.085 | 0.51 | 0.155 | 91.1678 |
| | 82.8840 | 100 | 0.085 | 0.51 | 0.155 | 83.1719 |
| | 80.2054 | 1000 | 0.085 | 0.49 | 0.155 | 80.2407 |
| $10^6$ | 263.4713 | 10 | 0.045 | 0.5 | 0.185 | 284.0065 |
| | 244.3668 | 100 | 0.045 | 0.47 | 0.195 | 259.8426 |
| | 236.7530 | 1000 | 0.045 | 0.47 | 0.195 | 248.5952 |

The column marked with (*) gives velocities at $b/L = 0.7$, for which no location is indicated.

on $Z = 0.5$ is observed for the first time. Deflection of isotherms above the fin reveals fluid motion toward the hot wall, as is more evident at $Ra = 10^6$ (Fig. 4a). Peak velocities for ascending flow ($V_{max}$) move toward the hot wall and toward the lateral fin edges as $Ra$ grows (Table 3). The buoyancy force generated by the fin causes this effect.

At $Ra = 10^6$ the regime is convective, as on $XY$ planes not intersecting the fin (not shown), thermal stratification and boundary layers appear. On $Z = 0.5$ thermal stratification is also seen (Fig. 4a), except within the fin where isotherms are nearly vertical. At this $Ra$ the flow adheres to the fin (Fig. 4b), therefore, it has less difficulty to reach the hot wall above it, as seen in Fig. 4a, where the thermal gradient at the hot wall above the fin is significant. Fig. 4b shows hints of a second flow loop above the fin, which does not appear at lower $Ra$, while the loop at the fin tip has greatly increased in size.

### 4.2. Effect of increases in $R_k$

The temperature within the fin becomes more uniform (and nearly equal to the base temperature) for $R_k = 1000$, $Ra = 10^6$ (Fig. 5a), due to heat conduction. Maximum horizontal and vertical velocities at the axes of the $Z = 0.5$ plane, which are representative of the intensity of cavity flow, undergo different changes with $R_k$. While $V_m$ consistently grows with $R_k$, because of the enhanced buoyancy induced by all the fin surfaces, $U_m$ changes only slightly (Table 2). $V_{max}$ values at the clearances near the hot wall decrease as $R_k$ grows, but their locations remain essentially unchanged (Table 3).

At $Ra = 10^6$, $R_k = 1000$ (Fig. 5a) the vertical temperature gradients are very high below the fin, but the horizontal gradients at the hot wall above the fin are still relatively low. Intense heating of the fluid sweeping the lower fin surface creates a high buoyancy force. The loop above the fin that was observed at lower $R_k$ is displaced to the right to merge with the loop in front of the fin (Fig. 5b). These views suggest that the effect of a high $R_k$, is to displace the flow away from the base surface and to increase the heat transfer contribution from the fin in comparison with that from the hot wall.

### 4.3. Effects of increases in fin width

The circulation cell at $b/L = 0.7$ is similar to the one described for the narrow fin. A wider fin blocks the flow

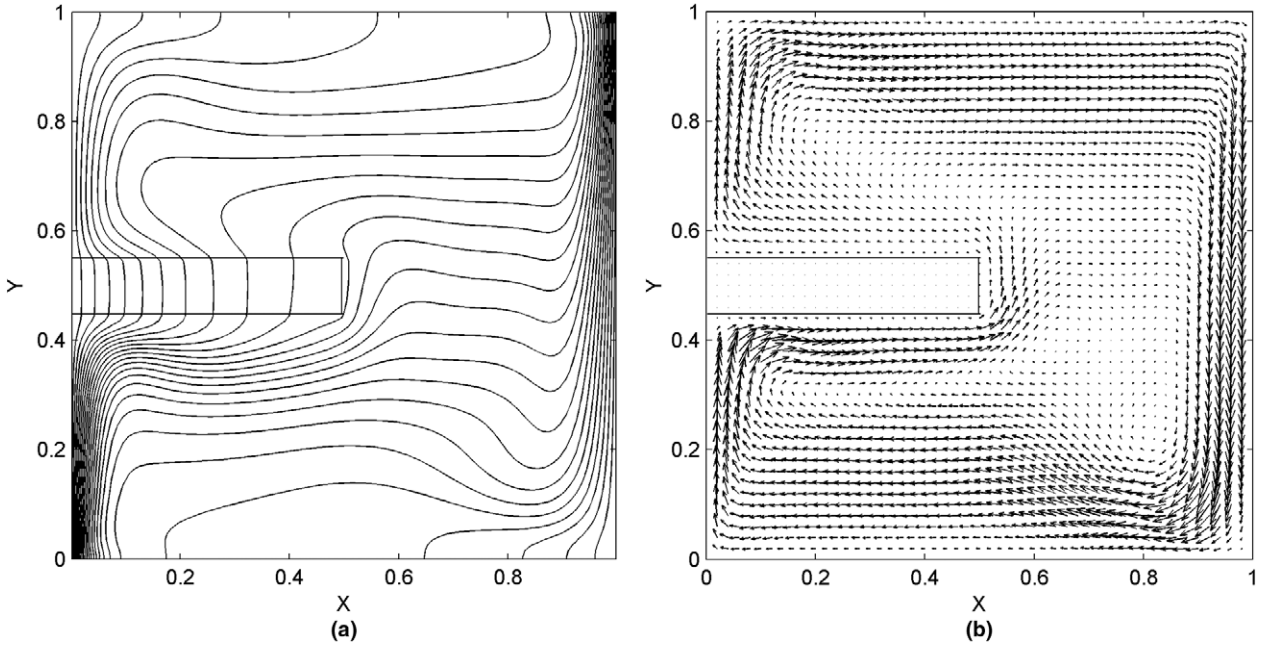


Fig. 4. Temperature and velocity fields on $Z = 0.5$, $Ra = 10^6$, $b/L = 0.5$, $R_k = 10$: (a) isotherms, (b) velocity vectors.

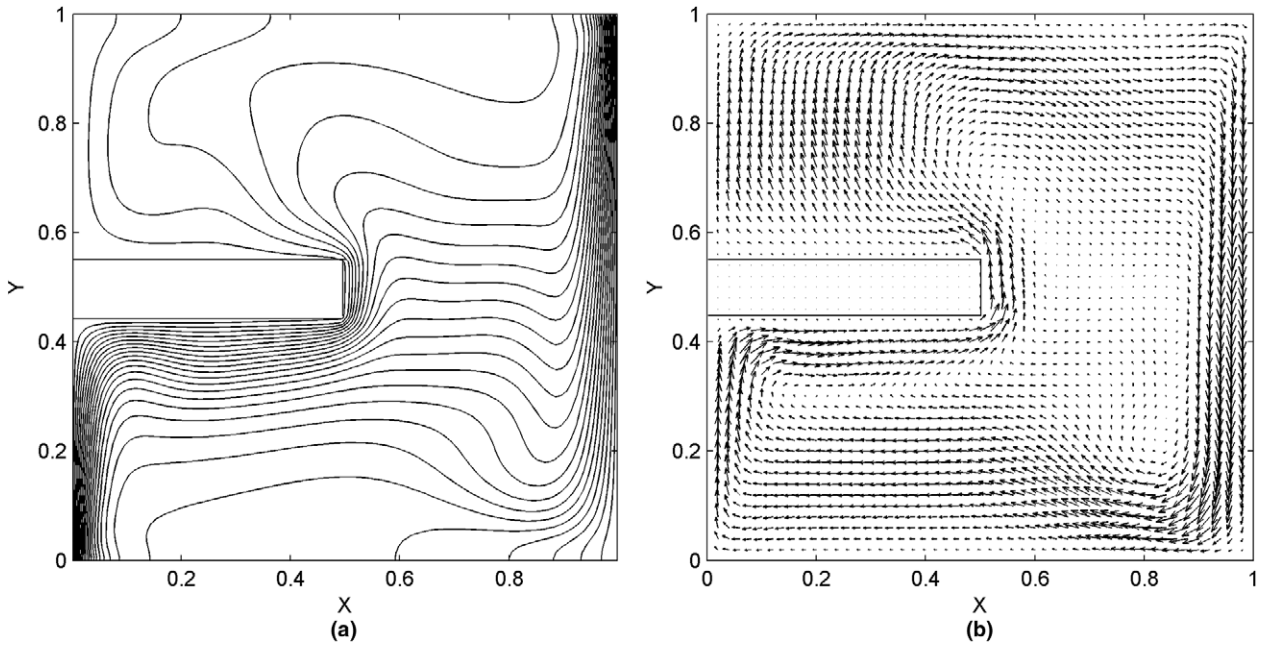


Fig. 5. Temperature and velocity fields on $Z = 0.5$, $Ra = 10^6$, $b/L = 0.5$, $R_k = 1000$: (a) isotherms, (b) velocity vectors.

more severely at the two lower Rayleigh numbers, as shown by a decrease in $V_{max}$ (Table 3). However, for the higher Rayleigh numbers this velocity undergoes a growth which, at $Ra = 10^6$, is significant. Simultaneously, $V_{max}$ decreases as $R_k$ increases, reflecting the displacement of the flow to the right at high $R_k$. Fig. 6a shows the ascending flow near the hot wall, at $Ra = 10^6$, $b/L = 0.7$, $R_k = 1000$. The velocities at the clearances are very high compared with those in the rest of the plane. The behaviour of the maximum velocities in the cavity axes is similar: While $U_m$ is reduced with respect to the narrow fin case at $Ra = 10^3$ and $10^4$, and $V_m$ increases marginally, both velocities grow with $b/L$ at the two highest Rayleigh numbers. Their increase is significant at $Ra = 10^6$ and high $R_k$. Another interesting feature is the definite flow that crosses the front fin edge toward the hot wall (Fig. 6b) while in the narrow fin this stream is rather weak, as implied by Fig. 5b. Globally, an increased fin width does not weaken the convective motion at high Rayleigh numbers, especially at high $R_k$.

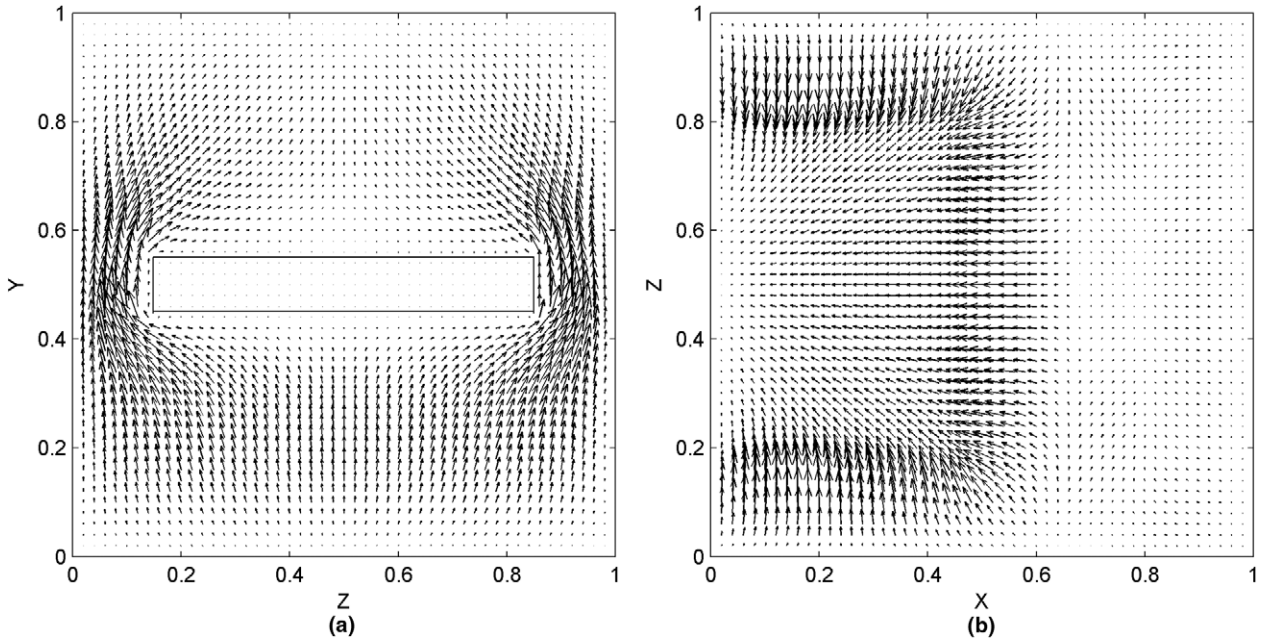


Fig. 6. Velocity vectors on two planes for $b/L = 0.7$, $Ra = 10^6$, $R_k = 1000$: (a) $X = 0.09$, (b) $Y = 0.585$.

### 4.4. Cavity heat transfer

Overall heat transfer rates for $b/L = 0.5$ and 0.7 are given in Tables 4 and 5. For a given fin width, $\overline{Nu}$ increases with $Ra$ and $R_k$, as expected. Heat transfer decreases with $b/L$, except at $Ra = 10^3$, where conduction is favoured by growths in the fin cross section. Also at $Ra = 10^6$ for the two high $R_k$ ratios, heat transfer grows slightly with $b/L$. This is explained by two facts: Firstly, as it will be shown, a higher $R_k$ increases the heat transfer contribution of the fin faces to the total heat transfer. Therefore, total heat transfer becomes less dependent on the heat transfer from the base surface. The heat transfer contribution from the bottom fin face increases with its area, compensating the relatively weak heat transfer from the base surface above the fin. Secondly, the top fin face is more effectively swept by flow coming from the front at high Rayleigh numbers, an effect that is enhanced for wider fins.

The relative heat transfer contributions of the hot wall and the fin faces are given in Table 6. As expected, the base surface accounts for the highest percentage of total cavity heat transfer. Its contribution increases with $Ra$, in response to a more intense convective regime. At a given $Ra$, the contribution of all fin faces grows with $R_k$, due to the higher temperature prevailing in the fin, which displaces the flow cell to the right. These growths occur at the expense of a reduction in the heat transfer contributed by the base wall, as supported by comparison of Figs. 4a and 5a. Table 6 shows that the frontal contribution is always important, in spite of its small area, because of the high temperature gradient at the fin tip. Table 6 also shows that the top fin face always transfers less heat than the bottom one, due to the difficulty for the fluid to reach the region above the fin. The bottom face contributes more heat, except in a single case. However, at $Ra = 10^3$ when conduction is dominant, the contributions of these faces become more similar with increases in $R_k$. For a purely conductive situation, the top and bottom faces would deliver equal heat transfer rates, as the temperature field would be symmetric about the horizontal midplane in absence of convection. A singularity is observed at $Ra = 10^4$, $b/L = 0.5$ and $R_k = 10$, where the upper fin surface is receiving heat from the fluid, as previously discussed in relation to Fig. 2a. In the $Ra = 10^6$ case the contributions of the top and bottom fin faces are nearly equal at $R_k = 10$. These contributions become dissimilar at higher $R_k$, in accordance with the very different temperature gradients observed above and below the fin in Fig. 5a.

Heat transfer enhancement, defined as the percent increase in $\overline{Nu}$ over the unfinned case at equal $Ra$, is shown in Table 7. At $Ra = 10^3$, in which the regime is essentially conductive, there are marked heat transfer enhancements in all cases. For the other Rayleigh numbers at $R_k = 10$, overall heat transfer is reduced at both fin widths, especially at $Ra = 10^4$. At this $Ra$, the lowering in circulation rate caused by fin blockage is severe, while the conductive contribution is limited by low thermal gradients in the fluid filled zones. The heat transfer reduction is more pronounced at $b/L = 0.7$, as the velocities are even lower owing to the blockage imposed by a wider fin, which further restricts the access of fluid to the hot wall above it. With $R_k$ ratios of 100 and 1000, heat transfer is enhanced, except at $Ra = 10^4$ with the wide fin. The highest heat transfer enhancement in convection dominated situations, slightly above 20%, occur at $Ra = 10^5$, $R_k = 1000$.

Table 4
Overall heat transfer results for a finned cavity, $b/L = 0.5$

| $Ra$ | $\overline{Nu}(R_k = 10)$ | $\overline{Nu}(R_k = 100)$ | $\overline{Nu}(R_k = 1000)$ |
|---|---|---|---|
| $10^3$ | 1.16692 | 1.38370 | 1.43831 |
| $10^4$ | 1.78080 | 2.2519 | 2.2889 |
| $10^5$ | 4.25581 | 4.96838 | 5.24441 |
| $10^6$ | 8.61241 | 9.63718 | 10.16473 |

Table 5
Overall heat transfer results for a finned cavity, $b/L = 0.7$

| $Ra$ | $\overline{Nu}(R_k = 10)$ | $\overline{Nu}(R_k = 100)$ | $\overline{Nu}(R_k = 1000)$ |
|---|---|---|---|
| $10^3$ | 1.20799 | 1.43623 | 1.50332 |
| $10^4$ | 1.63625 | 1.95275 | 2.16797 |
| $10^5$ | 4.07628 | 4.92484 | 5.23907 |
| $10^6$ | 8.49099 | 9.72051 | 10.29378 |

Table 6
Percent contributions to overall heat transfer from the hot wall and fin faces, $b/L = 0.5$

| $Ra$ | $R_k$ | Hot wall | Top | Bottom | Front | Sides |
|---|---|---|---|---|---|---|
| $10^3$ | 10 | 68.119 | 5.337 | 10.179 | 11.941 | 4.424 |
| | 100 | 35.725 | 15.779 | 20.776 | 17.183 | 10.537 |
| | 1000 | 28.766 | 17.933 | 23.006 | 18.157 | 12.138 |
| $10^4$ | 10 | 69.870 | −1.875 | 15.606 | 6.977 | 9.422 |
| | 100 | 43.686 | 6.758 | 26.128 | 11.900 | 11.528 |
| | 1000 | 35.983 | 9.803 | 27.888 | 13.942 | 12.384 |
| $10^5$ | 10 | 82.447 | 1.883 | 7.759 | 2.395 | 5.516 |
| | 100 | 60.967 | 5.830 | 18.136 | 5.891 | 9.176 |
| | 1000 | 54.696 | 6.948 | 20.995 | 7.058 | 10.303 |
| $10^6$ | 10 | 88.610 | 3.577 | 3.778 | 1.036 | 2.999 |
| | 100 | 70.734 | 5.863 | 12.865 | 3.547 | 6.991 |
| | 1000 | 63.694 | 6.783 | 16.255 | 4.808 | 8.460 |

### 4.5. Comparison with 2D case

Overall heat transfer rates for a square cavity with fins of the same length, thickness and $R_k$ of the 3D study are

Table 7
Heat transfer enhancement with respect to the unfinned case, percent

| $Ra$ | $b/L = 0.5$ | | | $b/L = 0.7$ | | |
|---|---|---|---|---|---|---|
| | $R_k = 10$ | $R_k = 100$ | $R_k = 1000$ | $R_k = 10$ | $R_k = 100$ | $R_k = 1000$ |
| $10^3$ | 8.93 | 29.17 | 34.27 | 12.77 | 34.07 | 40.33 |
| $10^4$ | −13.43 | 9.47 | 11.24 | −20.46 | −5.07 | 5.39 |
| $10^5$ | −2.24 | 14.13 | 20.47 | −6.37 | 13.13 | 20.34 |
| $10^6$ | −1.46 | 10.26 | 16.30 | −2.85 | 11.22 | 17.78 |

Table 8
Overall heat transfer in a square finned cavity

| $Ra$ | $\overline{Nu}(R_k = 10)$ | $\overline{Nu}(R_k = 100)$ | $\overline{Nu}(R_k = 1000)$ |
|---|---|---|---|
| $10^3$ | 1.25825 | 1.49962 | 1.54698 |
| $10^4$ | 1.57193 | 1.99001 | 2.08459 |
| $10^5$ | 3.79631 | 4.53000 | 4.74119 |
| $10^6$ | 8.24932 | 9.31246 | 9.72145 |

given in Table 8. This case may be considered representative of a fin covering the whole cavity width ($b/L = 1.0$), a case that was not run in this study in three dimensions, except for $Ra = 10^5$ and $10^6$. The highest heat transfer enhancement relative to the unfinned case in 2D, is 10%, at $Ra = 10^6$. Overall heat transfer rates in 2D are lower than in the three-dimensional cases, except at $Ra = 10^3$. Heat transfer reductions with respect to the $b/L = 0.5$ and 0.7 cases are most significant at $Ra = 10^4$ and $10^5$, and can be attributed to the absence, in the two-dimensional case, of a flow sweeping the base surface at fin-free spaces as it is possible in the 3D situation with a fin of partial width. The reduction is less significant, however, at $Ra = 10^6$. This is related to the fact that in the 3D case at high $Ra$, a significant stream originated at the front edge sweeps the top fin face. This kind of motion is similar to the only one allowed for access of fluid to the top fin face in the 2D case.

### 4.6. Maximum heat transfer rate

In this study, heat transfer enhancements of about 20% were obtained using relatively thick fins of high thermal conductivity. An asymptotic tendency to increases in $R_k$, implying that heat transfer would not grow significantly beyond $R_k = 1000$, is shown by tabulated results. Fins shorter than the ones considered here give lower heat transfer rates: because of their small area, their contribution to overall heat transfer at high $R_k$ is limited. Possibilities of heat transfer optimization can therefore be explored by varying the fin width. To quantify this, additional 3D runs were conducted varying $b/L$, keeping the other parameters at favourable values: $Ra = 10^5$, $R_k = 1000$ and $s/L = 0.5$ (Fig. 7). The lowest heat transfer rates occur at $b/L = 0$ (no fin) and at $b/L = 1$ (full fin width). Heat transfer increases steeply from both ends of the $b/L$ interval. The highest heat transfer rates occur in the zone $0.4 \leqslant b/L \leqslant 0.7$, with a maximum at $b/L = 0.6$, where the enhancement is 20.9%. The maximum results from the balance between the heat transfer contributions from the base wall and fin faces: Flow blockage with suppression of the stream that sweeps the hot wall at the clearances dominates in the full fin width case. The heat transfer contribution from the base area is low in this condition, but grows as the fin gets narrower. Meanwhile, the contribution from the fin faces is significant for wide fins but falls as the fin gets narrow. The enhancements provided by fins of partial width compare favourably with the ones obtained here with a full fin width, which only reach about 10% under favourable conditions.

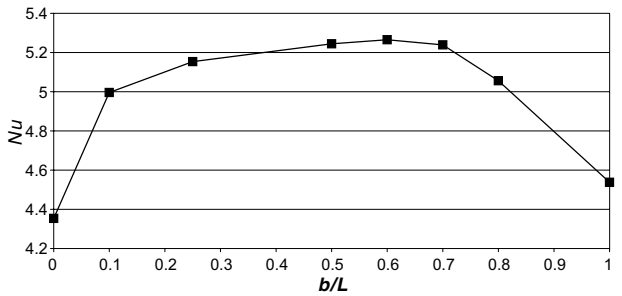


Fig. 7. Overall Nusselt numbers, $\overline{Nu}$ as a function of $b/L$, for $Ra = 10^5$, $R_k = 1000$.

To put this result in perspective, the same sensitivity analysis was done for $Ra = 10^6$. A maximum heat transfer rate, representing an 18% increase over the unfinned case, was found at $b/L = 0.8$. This result suggests that, as the maximum in heat transfer occurs for wider fins as $Ra$ grows, it would occur for the total fin width at even higher Rayleigh numbers.

## 5. Conclusions

In a numerical study of natural convection of air in a differentially heated cubical enclosure with a thick fin of partial width on the hot wall, the variation of overall Nusselt number with Rayleigh number, fin width and thermal conductivity ratio was investigated. A main circulation encompassing the whole cavity was found to govern the convective process. As the flow sweeps the fin faces and the hot wall, high velocities are reached at the clearances between the fin sides and the passive lateral walls. The fin inhibits the access of fluid to the upper fin face from its front and sides at low Rayleigh numbers. By increasing the thermal conductivity ratio, the cell is displaced away from the hot wall and the blockage effect is reduced.

Heat transfer reductions and enhancements with respect to the unfinned case are found at low and high $R_k$ respectively. Important enhancements, of about 20% are found at high $R_k$, caused by the combined contributions of the base wall and the fin faces. In the range of $Ra$ from $10^5$ to $10^6$, these contributions combine favourably to give a maximum heat transfer for particular fin widths. This effect can be of use in applications in which small cubical cavities are involved. However, at $Ra > 10^6$ the maximum heat transfer enhancement will occur for fins as wide as the cavity itself. In the upper Rayleigh number range of this investigation the heat transfer enhancements are found to be higher than the ones predicted in most two-dimensional studies.

## Acknowledgement

This study was supported by Fondecyt (project 1020106).

## References


Bejan, A., 1983. Natural convection in a porous layer with internal flow obstructions. Int. J. Heat Mass Transfer 26, 815–822.

Bilgen, E., 2005. Natural convection in cavities with a thin fin on the hot wall. Int. J. Heat Mass Transfer 48, 3493–3505.

da Silva, A.K., Gosselin, L., 2005. On the thermal performance of an internally finned 3D cubic enclosure in natural convection. Int. J. Therm. Sci. 44, 540–546.

De Vahl-Davis, G., 1983. Natural convection of air in a square cavity: a benchmark numerical solution. Int. J. Numer. Methods Fluids 3, 249–264.

Frederick, R.L., 1989. Natural convection in an inclined square enclosure with a partition attached to its cold wall. Int. J. Heat Mass Transfer 32, 87–94.

Frederick, R.L., Valencia, A., 1989. Heat transfer in a square cavity with a conducting partition on its hot wall. Int. Commun. Heat Mass Transfer 16, 347–354.

Lakhal, E.K., Hasnaoui, M., Bilgen, E., Vasseur, P., 1997. Natural convection in inclined rectangular enclosures with perfectly conducting fins attached on the heated wall. Heat Mass Transfer 32, 365–373.

Nag, A., Sarkar, A., Sastri, V.M.K., 1993. Natural convection in a differentially heated square enclosure with a horizontal partition plate on the hot wall. Computer Methods Appl. Mech. Eng. 110, 143–156.

Nag, A., Sarkar, A., Sastri, V.M.K., 1994. Effect of a thick horizontal partial partition attached to one of the active walls of a differentially heated square cavity. Numer. Heat Transfer, Part A 25, 611–625.

Oosthuizen, P.H., Paul, J.T., 1985. Free convection heat transfer in a cavity fitted with a horizontal plate on the cold wall. In: Shenkman, S.M. et al. (Eds.), Advances in Enhanced Heat Transfer—1985 ASME HTD 43.

Patankar, S.V., 1980. Numerical Heat Transfer and Fluid Flow. McGraw Hill, Hemisphere, Washington.

Scozia, R., Frederick, R.L., 1991. Natural convection in slender cavities with multiple fins attached to an active wall. Numer. Heat Transfer, Part A 20, 127–158.

Shi, X., Khodadadi, J.M., 2003. Laminar natural convection heat transfer in a differentially heated square cavity due to a thin fin on the hot wall. ASME J. Heat Transfer 125, 624–634.

Tasnim, S.H., Collins, M.R., 2004. Numerical analysis of heat transfer in a square cavity with a baffle on the hot wall. Int. Commun. Heat Mass Transfer 31, 639–650.

Tric, E., Labrosse, G., Betrouni, M., 2000. A first incursion into the 3D structure of natural convection of air in a differentially heated cubic cavity, from accurate numerical solutions. Int. J. Heat Mass Transfer 43, 4043–4056.

Yucel, N., Turkoglu, H., 1998. Numerical analysis of laminar natural convection in enclosures with fins attached to an active wall. Heat Mass Transfer 33, 307–314.